BUFFERED ACCELERATED WEATHERING OF LIMESTONE FOR STORING CO_2: CHEMICAL BACKGROUND

Stefano Caserini*[a], Giovanni Cappello[b], Davide Righi[a], Guido Raos[c], Francesco Campo[a], Serena De Marco[a], Phil Renforth[d], Selene Varliero[c], Mario Grosso[a]

a Dipartimento di Ingegneria Civile ed Ambientale, Politecnico di Milano, Milano, Italy

b CO2Apps, Galbiate (LC), Italy

c Dipartimento di Chimica, Materiali e Ingegneria Chimica "G. Natta", Politecnico di Milano, Milano, Italy

d The Research Centre for Carbon Solutions, Heriot-Watt University, Edinburgh, United Kingdom

Abstract

We present an evolution of the Accelerated Weathering of Limestone (AWL) method to store CO_2 in seawater in the form of bicarbonates. Buffered Accelerated Weathering of Limestone (BAWL) is designed to produce a buffered ionic solution, at seawater pH, which derives from the reaction between a CO_2 stream and a powder of micron-sized calcium carbonate particles in a long tubular reactor. Addition of calcium hydroxide to buffer the unreacted CO_2 before the discharge in seawater is also provided. BAWL aims to overcome the main limitations of AWL, such as the high amount of water needed, the large size of the reactor, the risk of CO_2 degassing back into the atmosphere, if the ionic solution is released into shallow waters, as well as the induced seawater acidification. This paper presents the chemical background of the technology and evaluates its feasibility by considering the chemical equilibria in the different phases of the process. The CO_2 emitted for limestone calcination leads to a 24% CO_2 penalty; a preliminary cost analysis assesses a storage cost of 100 € per tonne of CO2 from an external source. It finally discusses the main features to be considered for the design at the industrial scale.

Keywords: CO_2; Mitigation; CCS; Storage; Capture; Limestone; Ocean; Acidification.

1. INTRODUCTION

The continuous addition of fossil CO_2 into the atmosphere is drastically affecting the natural equilibrium of the global carbon cycle, warming the climate and acidifying the oceans. For this reason, a rapid decrease in greenhouse gasses emissions, albeit essential, is clearly not sufficient to limit global warming to "well below +2°C" with respect to the pre-industrial levels, as required by Article 2 of the Paris Agreement. A simultaneous and unprecedented effort of removing large quantities of CO_2 from the atmosphere is therefore urgently needed.

Carbon Capture and Storage (CCS) is one of the technological options studied for the decarbonisation of the energy sector and of many industrial processes. CO_2 storage is also essential for the development of Negative Emissions Technologies (NETs) such as Direct Air Capture (DAC) or Bio-energy with carbon capture and storage (BECCS), which aim to remove atmospheric CO_2 at the gigatons (Gt)-scale. The same applies to processes where CO_2 removal is indirectly obtained from the spreading of alkaline materials (i.e. calcium hydroxide, 'ocean liming') where process CO_2 generated during calcination should also be captured and stored (Harvey, 2008; Renforth and Henderson, 2017; Caserini et al., 2019; Rackley, 2020).

According to the International Energy Agency (IEA, 2014), it is of particular importance to boost activities in the area of CO_2 storage, at various levels, because storage is critical to any CCS project design and must be addressed up-front.

Among the storage options, geological storage is the most advanced one and has a large theoretical worldwide potential (Bui et al., 2018). Although it is already at a commercial level of development (GCCSI, 2019**)**, and is used today for Enhanced Oil Recovery (EOR) (Bui et al., 2018), it has several drawbacks. Firstly, it can take 5-10 years to qualify a new saline formation suitable for CO_2 storage, and even when theoretical estimates are already available and look promising, a large up-front investment is needed to secure storage capacity (IEA, 2014). Second, since the geographical distribution of the suitable locations is uneven (Global CCS Institute, 2019), geological storage requires concentrating CO_2 emissions sources in large clusters in order to minimise the logistic costs

(Ajayi et al., 2019**)**. It is thus important to develop alternative solutions that could provide permanent storage of large quantities of CO_2, especially where and when geological storage is not feasible.

Different methods for CO_2 storage have been studied (IPCC, 2005). Although direct CO_2 storage in the ocean (Adams et al., 1995; Adams and Caldeira, 2008) could sequester large quantities of CO_2 for many centuries, the risks of seawater acidification and the potential impacts on the marine environment limit its applicability. The storage of CO_2 in the form of bicarbonates has been proposed by Rau and Caldeira (1999), with a method called Accelerated Weathering of Limestone (AWL), consisting in the reaction of CO_2 from power plants exhaust gas with seawater and carbonate minerals ($CaCO_3$), calcite or aragonite, with a final discharge in the ocean of an ionic solution rich in bicarbonates. This method has progressed from the laboratory level (Rau, 2011) to the feasibility case study (Chou et al., 2015) and to a pilot-scale reactor (Kirchner et al., 2020a), as well as with modelling of local impacts on seawater carbonate chemistry (Kirchner et al., 2020b).

This paper proposes a new technology, called Buffered Accelerated Weathering of Limestone (BAWL), that can be considered as an evolution of the AWL, aimed at overcoming its main limitations: the high amount of water needed, the large reactor, the risk of CO_2 degassing back into the atmosphere if the ionic solution is released into shallow waters and the induced seawater acidification if the ionic solution is released in deep waters.

In Section 2 we introduce the BAWL technology and compare it with AWL. In Section 3 we discuss the model and numerical methods used to simulate the process, considering in particular the chemical kinetics for the dissolution of carbonate mineral particles. Sections 4 and 5 present and discuss our numerical results for some representative situations. The conclusions follow.

2. AWL AND BAWL

2.1. Accelerated Weathering of Limestone (AWL)

77 Rau and Caldeira (1999) proposed the AWL method for storing CO_2, where a CO_2-rich effluent gas
78 stream flows over or through a porous bed of limestone which is wetted by a continuous spray or
79 flow of water. High-CO_2 exhaust gas is conveyed through the reactor, where it enters into contact
80 with water and the wetted surfaces, forming carbonic acid that reacts in turn with the carbonate solid
81 (e.g. calcium carbonate) to produce HCO_3^- in solution. The net reaction is (Eq. 1):

82 $$CO_2(aq) + CaCO_3(s) + H_2O(l) \rightleftharpoons Ca^{2+}(aq) + 2HCO_3^-(aq) \qquad (1)$$

83 The same carbonate dissolution reaction occurs naturally on land and in the sea, but over the course
84 of millennia (Lord et al., 2016). AWL accelerates this natural process and leads to a permanent storage
85 of carbon as bicarbonates in the ocean, for a large fraction of CO_2 involved in the reaction. This type
86 of carbon storage is geochemically and environmentally advantageous, because the ocean already
87 contains an extraordinarily large amount of carbon, mainly in the form of dissolved bicarbonate. The
88 oceans carbon sink is one order of magnitude larger than that contained in all recoverable oil and coal
89 reserves and about 60 times higher than that present in the atmosphere. In addition, the only solid
90 reactant needed for the sequestration process, the carbonate mineral, is roughly 4,000 times more
91 abundant than the carbon contained in oil and coal deposits globally; its global availability is not a
92 limit to sequester gigatons of anthropogenic CO_2.
93 The main challenge that limits the feasibility of AWL is related to the poor solubility of the dissolving
94 minerals, and thus large water requirements, i.e. 1×10^4 m^3 $t_{CO2stored}^{-1}$ with the proposed reactor design
95 (Rau and Caldeira, 1999) and 3.8×10^3 m^3 $ton_{CO2stored}^{-1}$ with optimised future large scale reactors (Rau,
96 2011). The AWL reactor proposed by Rau and Caldeira is a standard limestone contactor used for
97 adding alkalinity to waters, namely a vessel, atmospheric or pressurised, where a CO_2-rich gas stream
98 enters by one or more entryways and then passes over or through a wetted, porous bed of limestone
99 particles within the reactor, operating updraft or downdraft (Rau and Caldeira, 1999). Rau (2011) and
100 Kirchner et al. (2020a) showed that completing the calcite dissolution requires large reactors and long
101 reaction times, i.e. from several hours up to weeks. This substantially increases the size and the cost
102 of the reactors.

Furthermore, the CO_2 storage efficiency is low if the ionic effluent is discharged into shallow waters, since the effluent released from the reactor has a high CO_2 partial pressure, which would result in either degassing of CO_2 into the atmosphere or in recirculating part of the CO_2 if the degassing is artificially induced prior to the discharge. On the contrary, if the ionic effluent is discharged into deep waters, the CO_2 storage efficiency is high, but at the expense of acidifying the sea.

Kirchner et al. (2020b) evaluated the performance of an AWL-reactor installed at a coal-fired power plant in Germany, and also simulated how AWL-derived water impacts the southern North Sea's shallow waters carbonate chemistry. They found that the discharge of the AWL-derived water could have a substantial effect on the marine biota if the release of the reactor outflow occurs in the absence of adequate advection/mixing conditions within the water body; this causes a significant alteration on pH and Ω_{cal} (saturation state of calcite), by 1 and 8 units respectively. A significant reduction of the CO_2 storage efficiency has been assessed, since approx. 50% of the captured CO_2 remained permanently stored in the North Sea, while the other 50% re-entered the atmosphere at the end of the experiments due to degassing and carbonate mineral precipitation.

2.2. Buffered Accelerated Weathering of Limestone (BAWL)

The new BAWL process aims to overcome the above-mentioned limitations of the AWL technology. The raw material for the BAWL is limestone, which is an abundant sedimentary carbonate rock mainly formed by calcite $CaCO_3$ (and to a smaller extent by $MgCO_3$). In this article, all the reactions and calculations are referred to pure calcite $CaCO_3$, but analogous reasonings apply to aragonite, dolomite or magnesite.

The BAWL process consists of four distinct elements (Figure 1):

- a mixer (MIX), where a CO_2 stream is mixed with the micronised carbonate mineral and seawater in order to form a carbonate-rich slurry. CO_2 is in stoichiometric excess with respect to calcium carbonate within the slurry exiting from the MIX;

- a dissolution reactor (DR), where the carbonate is dissolved into an ionic solution, according to reaction (1), during the flux towards the sea;
- addition, through a pipeline (slaked lime pipe, SL), of aqueous calcium hydroxide in a buffering reactor (BR), which corresponds to the final part of the DR. This is done in order to buffer the unreacted CO_2 remaining at the end of the DR, according to the following reaction (Eq. 2):

$$Ca(OH)_{2(aq)} + 2CO_{2(aq)} \rightleftharpoons Ca(HCO_3)_{2(aq)} \quad (2)$$

The ionic buffered solution, with the same pH as the surrounding seawater, is then released into the sea. The DR can be located anywhere, onshore or offshore on the seafloor of shallow or deep seas. If the DR is located offshore between the coast and the deep sea, the slurry that flows down the DR encounters a progressively increasing hydrostatic pressure that enhances the solubility of the carbonate minerals (Dong et al., 2018).

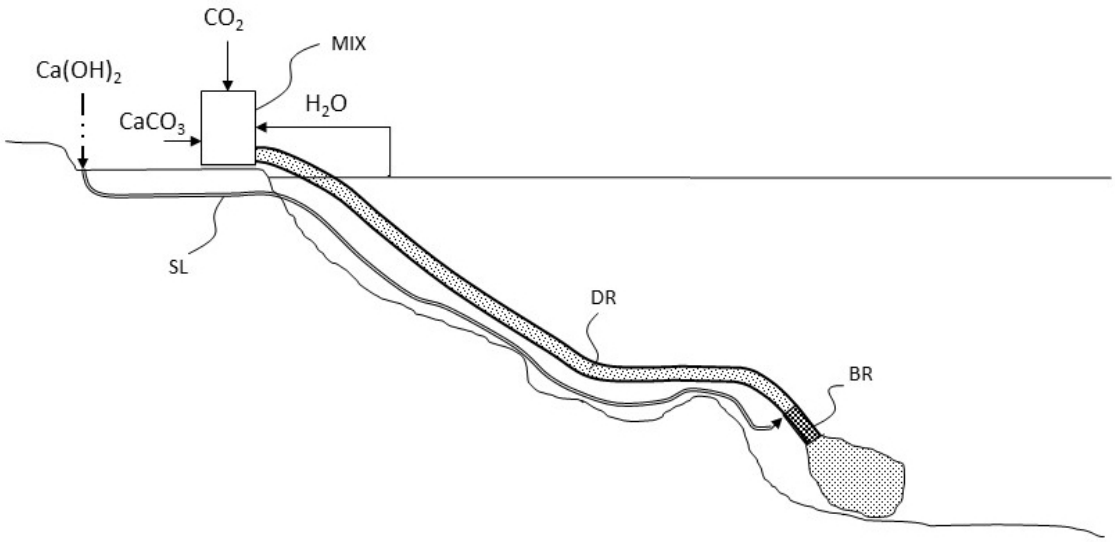

Figure 1: Configuration of BAWL. MIX: onshore mixer. DR: dissolution reactor; SL:– slaked lime pipe; BR: buffering reactor.

The quantity of carbonate fed to the MIX that could be completely dissolved before the end of the DR, in order to discharge into the sea a full ionic solution, is a function of the quantity of dilution

146 water used inside the DR, of the size of the carbonate particles, of the residence time and of the
147 pressure along the DR. The main objective of the DR is to maximise the amount of dissolved
148 carbonate per ton of CO_2. This requires the use of long residence times, high average pressure
149 (hundreds of bar in the deep seas), fine $CaCO_3$ particles (micron-size), and a fully turbulent flow in
150 the DR to prevent the sedimentation of the particles and to enhance the mixing of the reactants. The
151 solution at the end of the DR is acidic, since achieving the full dissolution of the $CaCO_3$ particles
152 requires a stoichiometric excess of CO_2. This solution can be buffered with $Ca(OH)_2$ within the BR,
153 to bring the pH back to that of natural seawater. The final buffering must be done in a way that avoids
154 the abiotic precipitation of the carbonate in the BR. According to Pytkowicz (1973) and Morse and
155 He (1993), no abiotic precipitation of calcium carbonate will occur in sea waters with Ω_{cal} below 20-
156 25, and the nucleation time needed to generate precipitation of carbonate in highly supersaturated
157 artificial seawater solutions is of several minutes or even hours (Pytkowicz, 1973).
158
159 **2.3. MIX**
160 In the MIX, the CO_2 stream (either contained in a flue gas or as a pure CO_2 stream previously
161 separated) is hydrated through a bubble-type absorption column (Figure 2) or a packed bed absorption
162 column. The column is formed by a vertical vessel, pressurised or atmospheric, where fresh seawater
163 is fed from its upper part, and the CO_2-rich gas is fed either through a bubble generator from its lower
164 part or directly to the vessel below the packing bed (Nock et al., 2014). The CO_2-depleted gas is
165 evacuated from the upper part of the vessel, and water with dissolved CO_2 is released from the bottom.
166 In order to dissolve it in water, the partial pressure of the CO_2 fed to the MIX (i.e., P_{CO2}) should be
167 kept above the CO_2 gas-liquid equilibrium partial pressure calculated by Henry's Law for any given
168 water flow. Water scrubbing is the most widely used method for removing CO_2 from biogas and
169 landfill gas (Nock et al., 2014). Absorption in a bubble-type reactor can be 3-10 times faster than in
170 a packed bed column, thereby allowing a significant reactor size reduction for a large amount of CO_2
171 to be captured (Teir et al., 2014). The main design parameters of the MIX and its efficiency should

be calculated on a case by case basis, as a function of seawater temperature and salinity, of the partial CO_2 pressure (P_{CO2}) in the inlet gas stream, of the types of packing bed or bubble generator and of the operative pressure P_{MIX} of the MIX.

The micronised $CaCO_3$, preferably in the form of a suspension, is added at the bottom of the MIX and uniformly mixed with the main water stream before entering the DR.

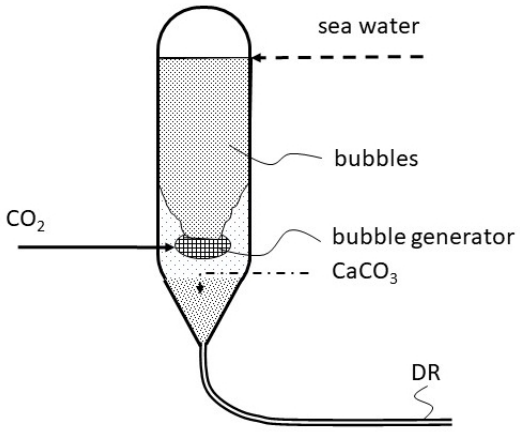

Figure 2: CO_2 hydration process in the MIX

2.4. DR-BR pipe

The DR could be manufactured with a commercially available HDPE pipe, that can reach an external diameter of up to 3500 mm (AGRU, 2021). Slurries with particle sizes below 50 µm are considered non-settling and form a homogeneous slurry (Plastic Pipe Institute, 2008). These fine particles remain in suspension, and for all practical purposes they become part of the carrier liquid, increasing its density. The particles' size considered in the present article is approx. 10 µm, so it is possible to assume that no settling will occur inside the DR, provided that a minimum velocity V_L of 1.2 m s^{-1} and a fully turbulent flow is maintained (Plastic Pipe Institute, 2008).

The BR section could be manufactured with the same material as the DR pipe, and it should be equipped with devices for a quick and effective mixing between the acidic solution flow coming from the DR and the stream of the buffering solution of $Ca(OH)_2$. The dispersion means could range from multiple nozzles to static mixers. A series of sensors placed at the exit of the BR should continuously

monitor the chemical characteristics (i.e. pH, alkalinity, hardness) of the final buffered ionic solution in order to feed the right amount of $Ca(OH)_2$.

The BR length depends on its capability to evenly mix the $Ca(OH)_2$ slurry with the acidic ionic solution released by the DR. The use of a static mixer leads to a BR length of approx. 5 times its diameter. The BR length is thus some dozens of meters, far shorter than the DR length (dozens of km).

2.5. SL-pipe

The SL pipe could also be manufactured in HDPE, and it can be parallel or coaxial to the DR pipe. The particles of slaked lime produced by the calcination of limestone forming the ionic solution of $Ca(OH)_2$ have a low diameter, well below 40 µm, so that the minimum flow rate speed limiting settling velocity could be easily achieved and calculated.

3. MATERIALS AND METHODS

3.1. Geochemical model

The simulations of $CaCO_3$ and CO_2 dissolution along the DR have been performed using the software PHREEQC Version 3, developed by the US Geological Survey (USGS, 2020) and designed to carry out a wide variety of aqueous geochemical calculations.

3.2.Seawater characteristics

Average values of seawater mineral composition, reported by Akinsola et al. (2012) and shown in Table SM.1 (Supplementary material), have been used in the calculation. The salt content in seawater, indicated by salinity (S) and defined as the amount of salt in grams dissolved in one kilogram of seawater, is 34.5 parts per thousand. This is within the salinity in the open ocean, typically ranging from about 34 to 37 parts per thousand (USGS, 2020).

The dissolution of $CaCO_3$ in water increases with increasing pressure and decreasing temperature (Shariatipuor et al., 2016). Seawater temperature depends strongly on the season and the location in the surface layers, but much less so at increasing depths [e.g., for depths > 100 m in the Mediterranean (Houpert et al., 2014)]. A constant average value of 10°C has been considered for all the calculations, as a first approximation. Pressure has been assumed to increase linearly with the depth, at a rate of 0.1 bar m^{-1}. Since an idealised linear slope of the pipe is considered, the weighted average pressure along a pipe reaching a depth *h* could be approximated to *h*/20 bar.

According to Sarmiento and Gruber (2006), seawater pH is typically between 7.5 and 8.4, with substantial regional and seasonal variations depending on temperature and salinity. For the calculations of this work, an initial seawater pH of 8, air-equilibrated with CO_2 at 420 ppm, has been considered for the input water that comes from shallow depth, whereas a seawater pH of 7.8 has been assumed for deep seawater. Within the typical range of the input seawater from shallow depth, the temperature of the water has a minor role in calcite dissolution, whereas other characteristics of the input seawater, such as pH and SI, are more relevant. A sensitivity analysis of the effect of these parameters, including also temperature and carbon saturation state, is outside the scope of the present work and will be developed in a subsequent article.

A comparison between SW characteristics at different depths calculated with PHREEQC and CO2SYS, another software widely used for calculating the state of the carbonate system of seawater (van Heuven et al., 2011) is shown in Table SM2. The two software speciation results make different predictions for the DIC (dissolved inorganic carbon) and its speciation. This indicates a difference in the calculated buffer capacity of natural seawater. Future work may also address the consequences of these differences for the operation of BAWL.

3.3. CO_2 hydration

The hydration of CO_2 in seawater is described by the following reaction (Eq. 3):

$$CO_{2(aq)} + H_2O_{(l)} \rightleftharpoons H_2CO_{3(aq)} \rightleftharpoons H^+_{(aq)} + HCO^-_{3(aq)} \quad (3)$$

The characteristic timescale for this process is less than one minute (Zeebe et al., 1999), far lower than the minimum residence time of the slurry inside the DR, between 14 and 40 hours. In other words, the kinetics of the reaction is not a limiting factor for the dissolution of calcite inside the DR. In the following it is assumed that $CO_{2(aq)}$ and $HCO_3^-{}_{(aq)}$ are always in equilibrium, and the overall reaction kinetics is assimilated to that of calcite dissolution. Because of the relatively high rate of reaction (3), and since the concentration of non-ionised carbonic acid ($H_2CO_{3(aq)}$) is small in comparison to that of $CO_{2(aq)}$ and $HCO_3^-{}_{(aq)}$, within PHREEQC the total aqueous amount of CO_2 (CO_2*) is considered as:

$$[CO_2^*] = [CO_2] + [H_2CO_3] \quad (4)$$

where $[X]$ denotes the molar concentration (mol kg^{-1}) of species X.

3.4. Calcite dissolution kinetics in DR

Calcite dissolution kinetics have been modelled using the rate equations originally proposed by Plummer et al. (1978), as implemented in the database of the PHREEQC software. The model adopts a standard expression of the rate equations, which applies to the bulk dissolution rates of many minerals. Palandri and Kharaka (2004) provide a brief introduction to such models, including some general guidelines about their applicability and limitations. In particular, the model by Plummer et al. (1978) was originally developed for calcite dissolution in freshwater. The salinity of seawater has been taken into account through the activity coefficients of the dissolved ions (see below). The reliability of the software and the underlying physical model has been assessed by Naviaux (2019), who compared the dynamics of calcite dissolution in seawater to the calculations using PHREEQC and other software. Naviaux (2019) concludes that PHREEQC underestimates the saturation state of calcite Ω_{cal}, defined as:

$$\Omega_{cal} = \frac{[Ca^{2+}][CO_3^{2-}]}{K'_{sp}} \quad (5)$$

where K'_{sp} is the stoichiometric solubility product of the $CaCO_3$ mineral in question (calcite in this

study). The saturation index of calcite is defined as $SI_{cal} = \log_{10} \Omega_{cal}$.

In PHREEQC the dissolution rate depends on the saturation index of $CaCO_3$, on the amounts of water and CO_2, on the pH of the solution and on the surface area index (*SAI*). The initial *SAI* depends on the size of the calcium carbonate particles, and then decreases as the reaction proceeds, since the particles decrease in size until they are completely dissolved. This is simulated in the software through an iterative process where the ratio between the initial surface area of calcite and the amount of substance left after each iteration is calculated with the following formula, proposed by Parkhurst and Appelo (2013):

$$A(t) = SAI(0)\, n(0) \left[\frac{n(t)}{n(0)}\right]^a \qquad (6)$$

where:

- *A(t):* surface area at time *t* (cm^2)
- *SAI(0)*: initial surface area index ($cm^2\ mol^{-1}$)
- *n(t)*: amount of calcite (mol) at time *t*
- *a*: an empirical exponent. (*a=0.6*)

The initial surface area index of calcite particles, *SAI*(0), depends on the mean particle size and can be calculated from the following equation, adapted from the work of Subhas et al. (2015):

$$SAI(0) = \frac{6}{\rho \cdot d} M_w \qquad (7)$$

where:

- $\rho = 2.63$ ($g\ cm^{-3}$) is the assumed density of calcite
- d : mean grain diameter (cm) of the sieved fraction.
- M_w : molar mass of $CaCO_3$ ($100.09\ g\ mol^{-1}$)

Calcite particles with 10 µm diameter have been considered, and this corresponds to a *SAI*(0) value of $2.28 \times 10^5\ cm^2\ mol^{-1}$.

292 Dissolution of calcite occurs through the following reactions, respectively prevailing at acidic, neutral
293 and alkaline pH:

294 $$CaCO_3(s) + H^+(aq) \overset{k_1}{\rightarrow} Ca^{2+}(aq) + HCO_3^- \quad (8)$$

295 $$CaCO_3(s) + H_2CO_3(aq) \overset{k_2}{\rightarrow} Ca^{2+}(aq) + 2HCO_3^- \quad (9)$$

296 $$CaCO_3(s) + H_2O(aq) \overset{k_3}{\rightarrow} Ca^{2+}(aq) + HCO_3^- + OH^-(aq) \quad (10)$$

297 The effect of each reaction on the dissolution rate is described by the model originally proposed by
298 Plummer, Wigley, Parkhurst (1978) and later adopted by several other authors (Shiraki and Brantley,
299 1995; Kaufmann and Dreybrodt, 2007):

300 $$R_f = k_1 a_{H^+} + k_2 a_{H_2CO_3*} + k_3 a_{H_2O} \quad (11)$$

301 where:

302 R_f: calcite dissolution rate, forward reaction (dissolution) (mol cm^{-2} s^{-1})

303 k_1, k_2 and k_3: temperature-dependent rate constants (mol cm^{-2} s^{-1})

304 a_X: thermodynamic activities of the species.

305 The reverse reactions describing calcite precipitation are modelled implicitly through a correction
306 term, depending on the calcite saturation state:

307 $$R_{net} = R_f(1 - \Omega_{cal}{}^{2/3}) \quad (12)$$

308 Alternatively, the precipitation could have been modelled explicitly through a fourth term in Eq.(11),
309 making a negative contribution to the rate. The adoption of one or the other calcite precipitation model
310 is irrelevant for this study, since the water inside the DR is always far from saturation when the calcite
311 dissolution kinetics is considered, as will be shown in the results section (see Table 1, Column C).
312 The thermodynamic activity of water is close to unity, while those of the solute species are related to
313 their molar concentrations, as follows:

314 $$a_X = \gamma_X[X] \quad (13)$$

315 where the activity coefficients γ_X depend on the temperature, salinity and pressure. All activities are
316 calculated by PHREEQC using the default program parameters.

317 The change in the amount of undissolved calcite (mol) can be calculated with Eq. 14:

318 $$\frac{dn(t)}{dt} = -A(t) \times R_{net}(t) \qquad (14)$$

319 The carbonate and calcium ions in solution change by an exactly opposite amount. Under turbulent
320 mixing conditions, such as those that exist within the DR, diffusion is not a limiting factor, and we
321 can equate the ion concentrations within the bulk solution to those close to the calcite surface. Then,
322 the calcite dissolution rate can be converted into a change in the concentration of the carbonate ion.
323 After each dissolution step, all the other solution equilibria are reassessed, in particular with respect
324 to water ionisation (pH) and the conversion of CO_2 to HCO_3^- [equation (3)].
325 Our PHREEQC code implementing the calcite dissolution model is provided in the Supplementary
326 Material (Table SM3).
327

328 **3.5. Example of BAWL working conditions**

329 Since an analytical calculation of the characteristics of the discharged effluent is not possible, because
330 of the non-linearity of the kinetics and the many parameters involved, we have assessed the water-
331 carbonate reactions involved in the BAWL process by numerical calculations on one representative
332 case. The following conditions are used as a proxy of a significant application case of the BAWL
333 technology:

334 - 1,000 kg (=22.7 kmol) of CO_2, coming from Steam Methane Reforming flue gas with 14%
335 CO_2 content, fed into the inlet of the bubbling column with a pressure higher than 2 bar, in
336 order to grant at least 0.28 bar pCO_2;
337 - 2,000 m^3 of seawater and 1,310 kg (=13.1 kmol) of micronised $CaCO_3$ (10 μm diameter) fed
338 in the onshore MIX together with the CO_2;
339 - a straight DR pipeline that goes from sea-level (0 m) to a depth of 3,000 m;
340 - a residence time of 100,000 s (28 hours); assuming 1m s^{-1} of seawater speed in the DR, this
341 corresponds to a DR length of approx. 100 km;

- 420 kg (=5.7 kmol) of $Ca(OH)_2$ are added in the BR in ionic form, diluted in 150 m^3 of seawater, to buffer the remaining CO_2 at the end of the DR.

The optimal values of reactants could be better defined in the design phase of the technology, also considering the cost of their supply, whereas other parameters such as the length of the pipeline and the discharge depth also depend on the geographical characteristics.

4. RESULTS

Based on the working conditions described in Section 3.5, Table 1 shows the calculated values of the following chemical properties of the solutions at the different stages of BAWL technology, as indicated in Figure 3:

- pCO_2: partial pressure of CO_2;
- TA: total alkalinity referred to the molar amount of bases in a solution that can be converted to uncharged species by a strong acid, given mainly by the sum of HCO_3^-, $2CO_3^{2-}$ and OH^-.
- DIC: dissolved inorganic carbon, or total carbon, the sum of all the CO_2, HCO_3^-, and CO_3^{2-} species plus their ion pairs and complexes.
- $CO_2(aq)$, HCO_3^-, CO_3^{2-} and Ca^{2+}: concentrations of the species, in μmol kg^{-1}.
- SI_{cal} and Ω_{cal}: respectively the saturation index and the saturation state of calcite, defined in Section 3.4.
- pH: negative of the base 10 logarithm of the activity of the H^+ ion, hydronium ions, protons bound to water molecules. PHREEQC result reported in Table 1 are in the NBS scale, at the in-situ temperature of 10°C.

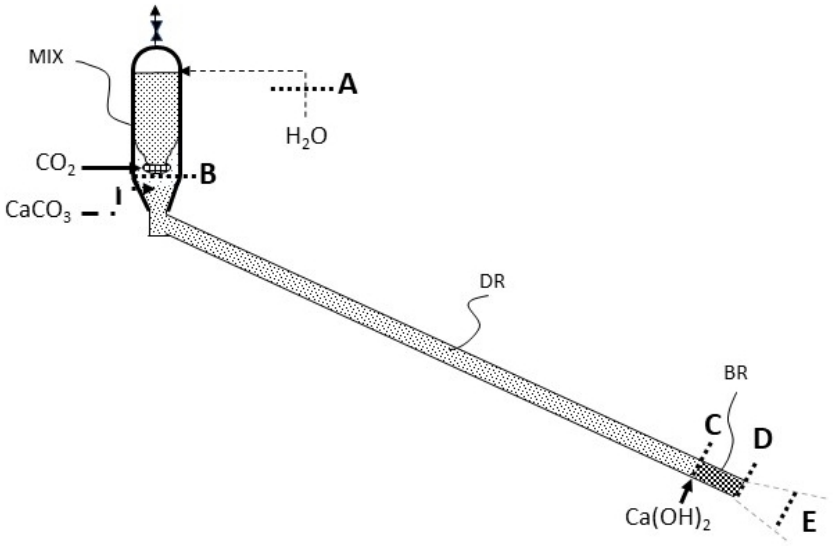

Figure 3: Main phases of the BAWL. A: Natural seawater. B: seawater in equilibrium with CO_2, before entering DR. C: end of DR, after reaction with $CaCO_3$. D: end of BR, after the reaction with $Ca(OH)_2$. E: plume discharged into the sea and diluted 20:1 with seawater.

Table 1: Calculated chemical properties at various steps of the BAWL process (for working conditions, see Section 3.5). All the concentrations are molalities (i.e., the mass in the denominator is that of pure water).

	Natural shallow water (A)	**Equilibrium after CO_2 addition (B)**	**End of DR – after reaction with $CaCO_3$(C)**	**End of BR - after reaction with $Ca(OH)_2$ (D)**	**Dilution 20:1 with deep seawater (E)**
pCO_2 (bar_a)	0.000420	0.28			
TA (µeq kg^{-1})	2,376	2,376	16,020	20,190	3,206
DIC (µmol kg^{-1})	2,327	13,920	20,740	19,460	3.195
$CO_{2(aq)}$ (µmol kg^{-1})	30	11,530	4,743	170	54
HCO_3 (µmol kg^{-1})	1,699	1,821	11,680	13,430	2,254
CO_3^{2-} (µmol kg^{-1})	18	0.05	5	190	16
Ca^{2+} (µmol kg^{-1})	9,297	9,304	15,240	16,860	9,760
SI_{cal}	0.37	-2.16	-0.23	1.38	0.05
Ω_{cal}	2.34	0.007	0.59	24	1.12
pH	8	5.5	6.5	8	7.8

The initial seawater is calculated in equilibrium with the atmosphere (column A), since it comes from shallow depth. The dissolution of CO_2 in the MIX will generate a carbonic acid solution with a pH of 5.5 (column B), which is highly corrosive to most common carbonate minerals. After $CaCO_3$ is added in the final part of the MIX, and the slurry enters the DR, at the end of the DR (column C) all

374 the $CaCO_3$ is dissolved in seawater, while a certain amount of CO_2 is still unreacted. A pH of 6.5
375 implies still acidic conditions.
376 The addition of $Ca(OH)_2$ in the BR to buffer the unreacted CO_2 will increase the pH of the discharged
377 water to 8 (column D), equal to that of natural seawater (column A). The saturation state Ω_{cal} is below
378 the maximum value of 25, so any abiotic calcium carbonate precipitation is avoided, as explained in
379 Section 4.2.
380 The plume formed by the discharge stream in the surrounding seawater (column E, dilution ratio
381 20:1) has a lower Ω_{cal}, thus further reducing the risk of calcium carbonate precipitation. The result is
382 a discharged ionic solution with the same pH as the surrounding seawater.
383

384 **4.1. Carbonate dissolution in the DR**

385 To understand the variation of the amounts of reactants needed under different working conditions,
386 the amounts of unreacted CO_2 and dissolved $CaCO_3$ in the DR have been assessed for different
387 residence time, from 60,000 to 120,000 s, and for discharge depth varying from 0 to 6000 m,
388 corresponding to a discharge pressure from 0 to 600 bar (Figure 4).
389 Since these results are referred to the use of 2000 m^3 of water per ton of CO_2 (see Section 3.5), the
390 results for 1500 m^3_{H2O} ton_{CO2}^{-1} and 2500 m^3_{H2O} ton_{CO2}^{-1} of seawater are shown in Figure SM 1-2 in
391 the Supplementary Materials.
392 The decrease of the size of the particles increases the carbonate dissolution rates. The maximum
393 amount that can dissolve increases by approx. 20% when the diameter changes from 10 μm to 2 μm,
394 as shown in Figure SM 3.
395

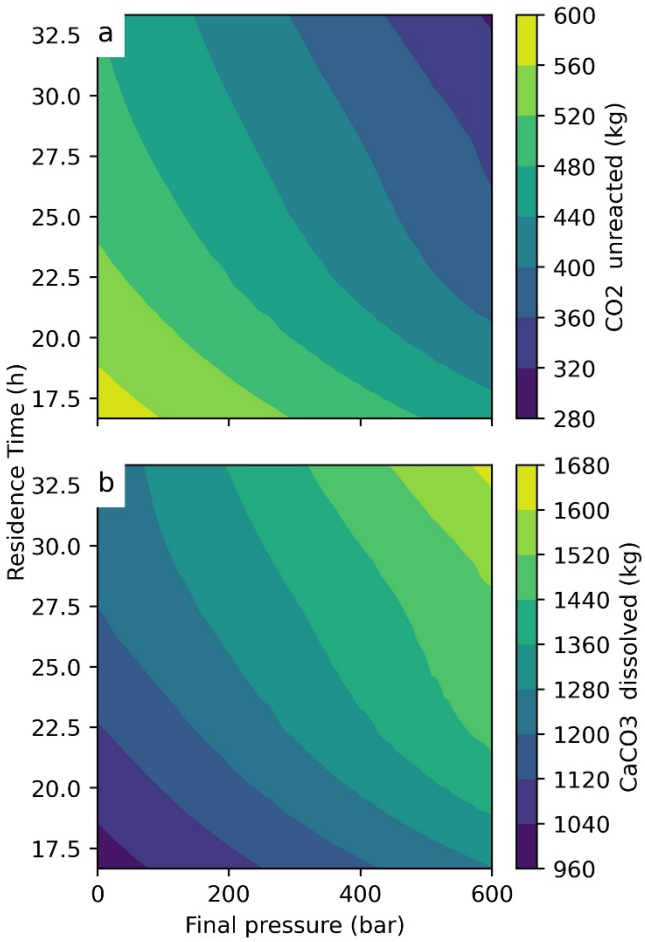

396

397 *Figure 4: Amount of unreacted CO_2 (a, top) and maximum amount of $CaCO_3$ that can dissolve (b, bottom) at the end of*
398 *the pipe for different residence times and different final pressures in the DR, considering 2,000 m^3 of seawater*

399 The results show that the maximum amounts of $CaCO_3$ that can dissolve will increase when the
400 residence time and the final pressure increase, and at the same time the unreacted CO_2 at the end of
401 the pipe will decrease. By increasing the pressure from 0 to 600 bar, the $CaCO_3$ that can dissolve in
402 seawater will increase by about 15%, and as a consequence the amount of CO_2 that remains unreacted
403 will decrease by 15%. By changing the residence time from 17 h to 22 h, the calcium carbonate that
404 dissolves in seawater would increase by 10%. As a consequence, the unreacted CO_2 at the end of the
405 pipe will decrease by approx. 5% from 17 h to 22 h, while it will reduce by approx. 2.5% for higher
406 residence times.

407

408 **4.2. Buffering with calcium hydroxide in BR**

409 The amount of calcium hydroxide that needs to be injected at the end of the DR to buffer the acidic
410 ionic solution in the BR, shown in Figure 5 together with the final Ω_{cal} at the discharge, depends on
411 the amount of unreacted CO_2 at point C. The results of the simulations with 1500 m^3_{H2O} ton_{CO2}^{-1} and
412 2500 m^3_{H2O} ton_{CO2}^{-1} of seawater are presented in Figure SM 4-5 (Supplementary Materials).
413 Although the reaction of SL with the seawater DIC in the SL pipe could lead to $CaCO_3$ the could
414 precipitation reduce the amount of $Ca(OH)_2$ that would be available for the reaction with the residual
415 CO_2 in the DR, this effect is limited to few percentage point of the SL used in the process.

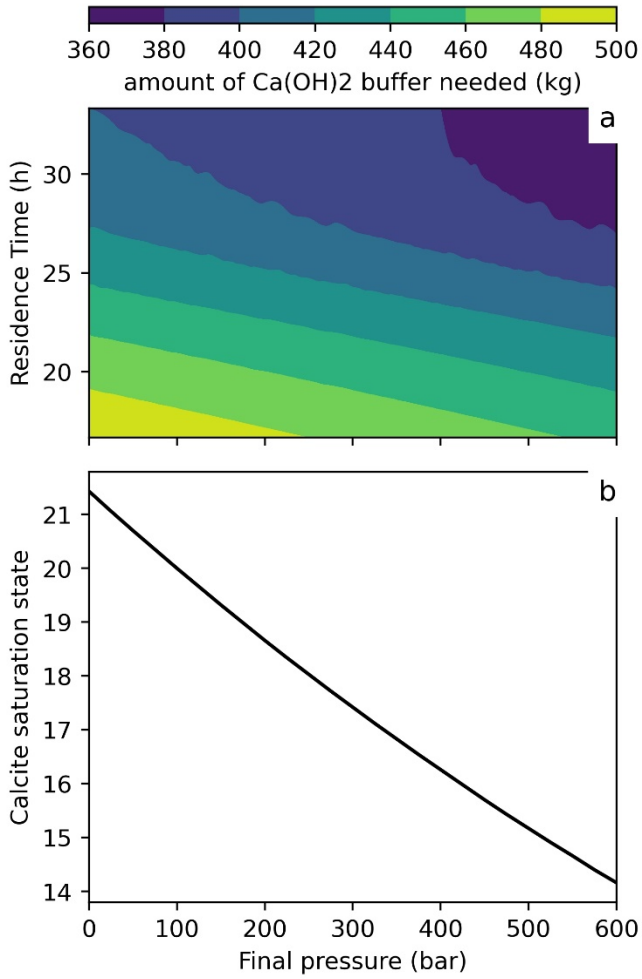

416

417 *Figure 5: Amount of $Ca(OH)_2$ needed to buffer the CO_2 entering the BR (a, top) and Saturation state after the buffering*
418 *(b, bottom) at the end of the BR, for different residence times and different final pressures, considering 2,000 m^3 of*
419 *seawater*

420 The amount of $Ca(OH)_2$ needed to buffer the solution will decrease as the residence time increases,
421 since the amount of $CaCO_3$ increases, as discussed in section 4.1. The saturation state Ω_{cal} does not

depend on the residence time inside the DR, but only on the final pressure, since all the reactants have been dissolved into ions, and the stoichiometric solubility product of $CaCO_3$ depends on the pressure (see reaction 5).

From 0 to 600 bar the amount of $Ca(OH)_2$ needed to buffer will decrease by 10%, while the saturation index will decrease by 8%. The increase of the residence time from 60,000 s to 80,000 s (16.7 to 22.2 hours) leads to the decrease of $Ca(OH)_2$ needed by 5%, for the same final pressures.

Overall, from 40% to 60% of the CO_2 used in the system is sequestered using $CaCO_3$, while the remaining amount is sequestered using $Ca(OH)_2$.

5. DISCUSSION

The final buffering of the unreacted CO_2 with slaked lime, that is the main difference between the AWL and the newly proposed BAWL, allows to release an ionic solution with the same pH of the seawater, thus avoiding acidification, as well as the risk of CO_2 degassing from seawater, that would otherwise reduce by 50% the CO_2 storage efficiency of AWL (Kirchner et al., 2020b). This improvement comes at the expense of an energy and CO_2 penalty, and thus at an increase in the cost of the process.

Another main difference between AWL and BAWL is the structure of the reactor: by using a tubular reactor, such as a submarine pipeline, it is possible to achieve long residence times, high reaction pressures, standardised and modular manufacturing, and a long-lasting and maintenance-free reactor. HDPE pipelines have a long lifetime (more than 100 years, according to Gabriel, 1999), and their submarine utilisation is a standard technology in waters up to 900 m deep (Pipelife, 2021); further engineering development is needed for laying the HDPE pipes in deeper waters.

The use of BAWL in deep waters allows higher efficiency, since deep waters favour the dissolution of the carbonates inside the DR, thus reducing the use of the more expensive slaked lime before the discharge of the ionic buffered solution into the sea. Furthermore, the Ω_{cal} of the buffered ionic solution also depends on the hydrostatic pressure at the end of the BR, and allows the use of less

448 dilution water inside the DR discharging into deep waters with a direct benefit on the DR investment
449 cost; the DR itself allows more CO_2 to be stored if installed in deep rather than in shallow waters. On
450 the other hand, the installation in deep water implies higher installation and monitoring costs.
451 Discharge depth will be a characteristic of any specific location and can be changed only partially.
452 Relevant is also the role of particle size, which could accelerate $CaCO_3$ dissolution but implies a
453 higher energy penalty for milling. The size of the $CaCO_3$ particle, their residence time in the pipeline
454 (i.e., the pipeline length) and the discharge depth should be chosen after a technical and economic
455 analysis that takes into account both the operative and capital cost of the installation (see section 5.2).
456 Although the injection of slaked lime in the BR, to buffer the remaining acidity, increases the
457 environmental acceptability of the discharge, it adds complexity to the process as well as energy and
458 CO_2 penalty. The BR should be carefully designed in order to allow a fast mixing between the slacked
459 lime slurry added and the ionic acid solution released by the DR, so as to avoid any possible
460 precipitation of the calcium and magnesium carbonate downstream the injection nozzles, where the
461 pH will increase. The use of proper mixing devices inside the BR, i.e. static mixers and multiple
462 nozzles generally used for the deacidification of waters with hydroxides, could shorten the mixing
463 process to a few seconds (Sulzer, 2021), thus avoiding prolonged situations of localised high pH that
464 can induce the precipitation of calcium carbonate. Chave and Suess (1970) demonstrated that even
465 increasing the Ω_{cal} by adding $CaCl_2$ to seawater, the precipitation of calcium carbonate would occur
466 only with very high pH levels, with time span ranging from several minutes to hours, after the
467 dissolved organic matter has been removed from the solution.
468 The kinetics and the conditions of $CaCO_3$ precipitation inside the BR, where the slaked lime is added,
469 should thus be investigated on a case by case basis, considering the presence of dissolved organic
470 carbon in the water and the calcium carbonate composition, since a higher Mg^{2+} content could inhibit
471 the calcium carbonate precipitation (Pytkowicz, 1973).
472

473 **5.1 Energy and CO_2 penalty**

474 The energy and CO_2 penalties of BAWL are mainly related to the supply of $CaCO_3$ and the production
475 of $Ca(OH)_2$.
476 For each tonne of CO_2 permanently stored in the ocean, about 1.31 tonne of limestone and 0.42 tonne
477 of $Ca(OH)_2$ should be dissolved in 2,000 tonne of seawater. The production of slaked lime implies a
478 further limestone consumption (0.56 tonne) and CO_2 emission (0.24 tonne for the calcination), thus
479 the amount of CO_2 that should be stored is larger than the amount of CO_2 that could come from an
480 external source (0.76 tCO_2), i.e. the production of H_2 with a SMR (steam methane reformer).
481 In the configuration used to evaluate the chemical equilibrium (see Table 1), almost 60% of the CO_2
482 reacts with $CaCO_3$ and 40% of the CO_2 reacts with $Ca(OH)_2$. It is worth noting that in the buffering
483 $Ca(OH)_2$ can react with more CO_2 than was emitted during its production, considering negligible the
484 further CO_2 produced during the overall process, to be assessed with a life-cycle approach.. Whereas
485 the production of 1 mole of $Ca(OH)_2$ from thermal calcination of $CaCO_3$ implies the production of 1
486 mole of CO_2, theoretically 1 mole of $Ca(OH)_2$ reacts with 2 mols of CO_2 according to the previous
487 reaction (2); in the PHREEQC simulations, only 1.5 – 1.8 moles of CO_2 react instead of 2 moles,
488 depending on the pressure and seawater characteristics.
489 The overall efficiency of the process should be evaluated through a life-cycle assessment that
490 considers the overall impact of the energy and material consumption for mining, transporting, milling
491 the required mineral, as well as the energy for limestone calcination and for pumping the needed
492 amount of seawater. As an example, the use of fossil energy for calcination implies further CO_2
493 emission and thus a decrease in the efficiency. In order to optimise the process, the electric energy
494 used to produce the $Ca(OH)_2$ and to mill the $CaCO_3$ should come from renewable sources. With the
495 working condition presented in section 3.5, the electric energy consumption for the process, mainly
496 for micronising the $CaCO_3$ and calcination process, is 1,152 kWh-e for each tonne of CO_2 stored
497 coming from an external source (See Table SM4).
498
499 **5.2 Preliminary economic evaluation**

Although a detailed evaluation of the costs and the design of an economically-optimised BAWL process is outside the scope of this paper, a preliminary calculation of the cost is reported in Table 2 for a reference plant with the biggest commercial HDPE pipeline (3.5 m diameter), for a total CO_2 storage of 156 kt y^{-1} and a net storage of 117 kt y^{-1} of CO_2 coming from an external source.

An electricity cost of 31 € MWh^{-1} has been considered based on the average current levelized cost of utility-scale photovoltaic and wind electricity (Lazard, 2021). The assumed limestone cost, 4 € ton^{-1}, is fairly in line with the values considered in previous analyses (Rau and Caldeira 1999; Rau et al., 2007; Harvey, 2007; Langer et al., 2009; Renforth et al., 2013) and with the average US cost for cement manufacturing in 2017 (USGS, 2021), whereas the transport cost is calculated considering an average supply distance of 500 km and 0.003 € ton^{-1} km^{-1} (Rau et al., 2007; Harvey, 2007; Langer et al., 2009). Labour cost, 29 € $hour^{-1}$, is the average European Union labour cost in 2020 (Eurostat, 2021).

The main component of the capital cost, the DR pipeline, has been calculated (**see Table SM5**) and explained considering HDPE, ballast and installation costs and assuming a 100-year lifetime; 40 years lifetime has been assumed for the other CAPEX components. An interest rate of 1.5% has been considered, taking into account the reference level of risk premia for decarbonisation investment in the EU (Alexandri et al., 2018).

The BAWL cost, that includes the cost of CO_2 capture from the flue gas and the subsequent storage, is assessed at about 74 € per tonne of CO_2 stored; considering the CO_2 penalty of the process due to the CO_2 emitted for calcination (24%), the cost for the storage of a tonne of CO_2 coming from an external source is about 100 € t^{-1}. This cost is within the range of the cost assessed for the AWL technology (18-128 \$ tCO_2^{-1}; Rau and Caldeira, 1999) and of CCS costs in current projects as Northern Light (Killingland et al., 2020). A more detailed assessment should consider the possibility of reducing the cost through the optimisation of the configuration, (i.e. considering different DR pipeline size and length, depth of the discharge, $CaCO_3$ particles diameter) as well as carefully evaluating the role of external variables such as the cost of electricity or limestone.

Table 2: Preliminary cost analysis

		Unit	Unit/year	€/unit	M€/year	€/tCO_2 stored	€/tCO_2 external source
OPEX	Electric energy	MWh	129,429	31	4.0	26	34
	Limestone stone	tonne	288,841	4.0	1.2	7.4	10
	Limestone transport	tonne	288,841	1.5	0.43	2.8	4
	Labour cost	hour	28,800	29	0.84	5.4	7
	Others (25% labour cost)				0.21	1.3	1.8
	OPEX total				6.6	43	57
CAPEX[1]	DR + SL pipeline				3.5	22	30
	Compressors and pumps				0.11	0.73	0.98
	Limestone Mill				0.039	0.25	0.3
	Calciner + slaker				0.11	0.73	1.0
	Mix				0.067	0.43	0.57
	Engineering & Construction (10%)				0.046	0.29	0.39
	CAPEX total				3.8	25	33
Contingency & Others (25% CAPEX)					1.0	6.2	8.2
TOTAL COST					11	74	98

[1] Considering 1.5% interest rate and 40 years lifetime, except 100 year for DR + SL pipeline

5.3 Environmental impacts

The discharge by BAWL has a high alkalinity content, which would increase the oceanic buffer capacity, whereas the high DIC level decreases this effect (Middelburg et al., 2020; Renforth and Campbell, 2021).

The ecological impact of localised increases of alkalinity remains poorly understood, and should be investigated further. Some works suggest an increase in calcification rates for coastal macro algae (Gore et al., 2019), but this has limited applicability at km injection depths. Adverse environmental impacts could be fully or partially mitigated by modifying the carbonate chemistry at the BAWL outflow (more or less alkalinity), or discharging in locations where there are higher mixing conditions in the water column or where stronger currents favour the dispersion.

Long DR pipe allows discharging the buffered ionic solution very far from coastal areas and in deep seawater, thus avoiding both the interference between the outflow and the fresh seawater needed for the process, and the interferences with the upper seawater levels, where most of the biological production and commercial fisheries occur (Herzog, 1998). On the contrary, the discharge in shallower waters (i.e. 100-1000 m) implies an easier and cheaper installation of the pipeline, and favour interaction of the high-alkalinity discharge with the ocean layers most affected by acidification.

$CaCO_3$ used for BAWL could have Mg and trace metals as impurities. Bach et al. (2019) assessed the potential consequences of high concentration of Mg on pelagic communities, and concluded that there is a low potential to induce positive and/or negative side effects. Trace metals occur at relatively low concentrations in seawater so that eventual perturbations at the scale of BAWL are likely sufficient to have a fertilising and/or toxic effect on organisms (Bach et al., 2019). Further research should focus on the potential impact of limestone impurities on the marine environment, as well as on the harmful substances that could be absorbed during the scrubbing in the MIX of the flue gas from a combustion source, like for AWL. The latter risk could be avoided, e.g. if the CO_2 comes from a pure stream previously separated from flue gas or from an electric calcinator.

6. CONCLUSIONS

The paper demonstrates the feasibility of using BAWL as a permanent CO_2 storage technology from a chemical perspective. BAWL could represent a solution where more developed CO_2 storage technologies are not an option, i.e. for emissions sources located in coastal areas, where geological formations suitable for CO_2 injection are not available, or where the logistic of transporting CO_2 to geological storage is too complex, or too expensive.

A very relevant positive aspect of this method is that the storage could be considered permanent over a very long timescale (Caldeira and Rau, 2000); the potential localised impacts of the high-alkalinity

565 discharge and of possible impurities found in $CaCO_3$ (i.e. trace metals) should be the focus of further
566 researches.
567 The use of a BAWL reactor for storing CO_2 in seawater in the form of bicarbonates moves the focus
568 from the technical problem of designing huge reactors onshore and from the efficiency/acidification
569 challenges of an AWL process, to the economic evaluation of the availability of carbonate deposits,
570 to the cost of renewable electric energy and to the logistic and the installation cost of long pipelines
571 in the deep sea.
572 A detailed techno-economic assessment of BAWL is currently being developed, along with a life
573 cycle assessment in order to evaluate the overall benefits and costs of this technology. Further
574 research is also needed to assess its feasibility as a large-scale option, to be used for H_2 production
575 through SMR (in the first phase) or for CO_2 removal (in a second phase), as well as the related
576 political, social, and environmental challenges, mainly due to the mining of large amounts of
577 limestone and to the impurities potentially discharged in seawater together with bicarbonates.
578

579 **7. REFERENCES**

580 Adams, E., Caldeira, K. (2008) Ocean Storage of CO2. Elements, 4, 319-324. doi:
581 10.2113/gselements.4.5.319
582 Adams, E., Golomb, D., Herzog, H. (1995) Ocean disposal of CO2 at intermediate depths. Energy
583 Conversion Management, 36, 447-452. doi: 10.1016/0196-8904(95)00041-B
584 AGRU (2021) Kunststofftechnik Gesellschaft m.b.H. Retrived January 27, 2021, from
585 www.agru.at/
586 Ajayi, T., Gomes, J., Bera, A. (2019) A review of CO_2 storage in geological formations
587 emphasising modeling, monitoring and capacity estimation approaches. Petroleum Science, 16,
588 1028-1063. doi: 10.1007/s12182-019-0340-8

589 Akinsola, O. E., Fatokun, A. O., Ogunsanmi, O. E. (2012) Investigation of salinity Effect on
590 Compressive Strength of Reinforced Concrete. Journal of Sustainable Development, 16, 74-82.
591 doi: 10.5539/jsd.v5n6p74
592 Alexandri E., Fragkos P. Lewney R. Paroussos L. (2018) A technical analysis on decarbonisation
593 scenarios - constraints, economic implications and policies. Technical Study on the
594 Macroeconomics of Energy and Climate Policies. Report by Cambridge Econometrics and E3-
595 Modelling for the European Commission
596 https://ec.europa.eu/energy/sites/ener/files/documents/technical_analysis_decarbonisation_scen
597 arios.pdf
598 Bach, L. T., Gill, S. J., Rickaby, R. E., Gore, S., Renforth, P. (2019) CO_2 removal with enhanced
599 weathering and ocean alkalinity enhancement: potential risks and co-benefits for marine
600 pelagic ecosystems. Frontiers Climate, 1, 7. doi: 10.3389/fclim.2019.00007
601 Bui, M., Adjman, C., Bardow, A., Anthony, E., Boston, A., Brown, S., et al. (2018) Carbon capture
602 and storage (CCS): the way forward. Energy & Environmental Science. doi:
603 10.1039/c7ee02342a
604 Caldeira, K., Rau , G. (2000) Accelerating carbonate dissolution to sequester carbon dioxide in the
605 ocean: Geochemical implications. Geophysical Research Letters, 27 (2), 225-228. doi:
606 10.1029/1999GL002364
607 Caserini, S., Barreto, B., Lanfredi, C., Cappello, G., Ross Morrey, D., Grosso, M. (2019)
608 Affordable CO_2 negative emission through hydrogen from biomass, ocean liming, and CO_2
609 storage. Mitigation and Adaptation Strategies for Global Change, 24, 1231-1248. doi:
610 10.1007/s11027-018-9835-7
611 Chave, K. E., Suess E. (1970) Calcium carbonate saturation in seawater: Effects of dissolved
612 organic matter. Limnol. Oceanogr. 15: 633-637.
613 Chou, W.-C., Gong, G.-C., Hsieh, P.-S., Chang, M.-H., Chen, H.-Y., Yang, C.-Y., et al. (2015)
614 Potential impacts of effluent from accelerated weathering of limestone on seawater carbon

615 chemistry: A case study for the Hoping power plant in northeastern Taiwan. Marine Chemistry,
616 168, 27-36. doi: 10.1016/j.marchem.2014.10.008
617 Dong, S., Subhas, A., Rollins, N., Naviaux, J., Adkins, J., Berelson, W. (2018) A kinetic pressure
618 effect on calcite dissolution in seawater. Geochimica et Cosmochimica Acta, 238, 411-423.
619 doi: 10.1016/j.gca.2018.07.015
620 Eurostat (2021) Hourly labour costs. https://ec.europa.eu/eurostat/statistics-
621 explained/index.php?title=Hourly_labour_costs
622 Gabriel, L. H. (1999) The Complete Corrugated Polyethylene Pipe Design Manual and Installation
623 Guide.
624 GCCSI (2019) Global Status of CCS 2019. Global CCS Institute
625 Gore, S., Renforth, P., and Perkins, R. (2018). The potential environmental response to increasing
626 ocean alkalinity for negative emissions. Mitig. Adapt. Strat. Glob. Change, 24, 1191–1211. doi:
627 10.1007/s11027-018-9830-z.
628 Harvey, L. (2008) Mitigating the atmospheric CO2 increase and ocean acidification by adding
629 limestone powder to upwelling regions. Journal of Geophysical Research, 113. doi:
630 10.1029/2007JC004373
631 Herzog, H. J. (1998) Ocean Sequestration of CO_2 - An Overview. Fourth International Conference
632 on Greenhouse Gas Control Technologies.
633 L. Houpert, P. Testor, X. Durrieu de Madron, S. Somot, F. D'Ortenzio, C. Estournel, H. Lavigne
634 (2014) Seasonal cycle of the mixed layer, the seasonal thermocline and the upper-ocean heat
635 storage rate in the Mediterranean Sea derived from observations. Oceanography 132 (2015)
636 333–352. doi: 10.1016/j.pocean.2014.11.004
637 IEA (2014) CCS 2014 What Lies in Store for the CCS? International Energy Agency.
638 IPCC (2005) IPCC special report on Carbon Capture and Storage. www.ipcc.ch

639 Kaufmann, G., Dreybrodt, W. (2007) Calcite dissolution kinetics in the system $CaCO_3$-H_2O-CO_2 at
640 high undersaturation. Geochimica et Cosmochimica Acta , 71, 1398-1410. doi:
641 10.1016/j.gca.2006.10.024
642 Killingland M., Krogh Boge M., Magneschi G. (2020) Potential for reduced costs for carbon
643 capture, transport and storage value chains CCS. The Norwegian Full-Scale CCS
644 Demonstration Project. DNV GL Energy Energy Markets and Technology, Report: 2019-1092,
645 Rev. 2. https://ccsnorway.com/wp-content/uploads/sites/6/2020/07/Report-Cost-reduction-
646 curves-for-CCS-Gassnova-version-2b-1.pdf
647 Kirchner, J., Berry, A., Ohnemuller, F., Schnetger, B., Erich, E., Brumsack, H.-J., et al. (2020a)
648 Reducing CO_2 Emission of a Coal-Fired Power Plant via Accelerated Weathering of
649 Limestone: Carbon Carture Efficiency and Environmental Safety. Environmental Science &
650 Technology. doi: 10.1021/acs.est.9b07009
651 Kirchner, J., Lettmann, K., Schnetger, B., Wolff, J.-O., Brumsack, H.-J. (2020b) Carbon Capture
652 via accelerated weathering of limestone: Modelling local impacts on the carbonate chemistry of
653 the southern North Sea. International Journal of Greenhouse Gas Control, 92, 1-10. doi:
654 10.1016/j.ijggc.2019.102855
655 Langer W.H., San Juan C.A., Rau G.H. Caldeira K. (2009) Accelerated weathering of limestone for
656 CO2 mitigation: opportunities for the stone and cement industries. Mining Engineering
657 61(2):27-32
658 Lazard (2021) Levelized Cost of Energy Analysis, version 14.0.
659 www.lazard.com/perspective/levelized-cost-of-energy-and-levelized-cost-of-storage-2020/
660 Lord, N. S., Ridgwell, A., Thorne, M. C. and Lunt D. J. (2016), An impulse response function for
661 the “long tail” of excess atmospheric CO2 in an Earth system model, Global Biogeochem.
662 Cycles, 30, 2–17, doi:10.1002/2014GB005074.
663 Middelburg J.J., Soetaert K., Hagens M. (2020) Ocean Alkalinity, Buffering and Biogeochemical
664 Processes. Review of Geophysics, 58, doi: 10.1029/2019RG000681

665 Millero F. J. (2007) The Marine Inorganic Carbon Cycle. Chem. Rev., 107 (2), 308–341.
666 https://doi.org/10.1021/cr0503557
667 Morse, J. W., He, S. (1993) Influences of T,S and PCO_2 on the pseudo-homogeneous precipitation
668 of $CaCO_3$ from seawater: implications for withing formation. Marine Chemistry, 41, 291-297.
669 doi: 10.1021/cr050358j
670 Naviaux, J. D. (2019) Chemical amd Physical Mechanism of Calcite Dissolution in Seawater, Ph.D
671 Thesis, California Institute of Technology.
672 Nock, W. J., Walker, M., Kapoor, R., Heaven, S. (2014) Modeling the Water Scrubbing Process
673 and Energy Requirements for CO_2 Capture to Upgrade Biogas to Biomethane. Industrial &
674 Engineering Chemistry Research, 53 (32), 12783-12792. doi: 10.1021/ie501280p
675 Palandri, J. L., Kharaka, Y. K. (2004) A Compilation of Rate Parameters of Water-Mineral
676 Interaction Kinetics for Application to Geochemical Modelling. US Geological Survey.
677 Parkhurst, D., Appelo, C. (2013) Description of Input and Examples for PHREEQC Version 3 - A
678 computer Program for Speciation, Batch-Reaction, One-Dimensional Transport, and Inverse
679 Geochemical Calculations. USGS.
680 Pipelife (2021) Retrieved January 27, 2021, from pipelife.com.
681 Plastic Pipe Institute (2008) Second edition handbook of PE pipe 2008.
682 https://plasticpipe.org/publications/pe-handbook.html
683 Plummer, L., Wigley, T., Parkhurst, D. (1978) The kinetics of calcite dissolution in CO_2-water
684 systems at 5°C to 60°C and 0.0 to 1.0 atm CO_2. American Journal of Science, 278, 179-216.
685 doi: 10.106/0009-2541(85)90024-5
686 Pytkowicz, R. M. (1973) Calcium carbonate retention in supersaturated seawater. American Journal
687 of Science, 273, 515-522. doi: 10.2475/ajs.273.6.515
688 Rackley, S. (2020) Ocean Alkalinity Enhancement A preliminary research agenda and maturation
689 roadmap. CarbonActionNow!

690 Rau, G. H. (2011) CO_2 Mitigation via Capture and Chemical Conversion in Seawater.
691 Environmental Science & Technology, 45, 3, 1088–1092. doi: 10.1021/es102671x
692 Rau, G., Caldeira, K. (1999) Enhanced carbonate dissolution: a means of sequestering waste CO2
693 as ocean bicarbonate. Energy Conversion & Management, 1803-1813. doi: 10.1016/S0196-
694 8904(99)00071-0
695 Rau, G., Knauss, K., Langer, W., & Caldeira, K. (2007) Reducing energy-related CO_2 emissions
696 using accelerated weathering of limestone. Energy, 32, 1471-1477. doi:
697 10.1016/j.energy.2006.10.011
698 Renforth P., Jenkins B.G., Kruger, T. (2013) Engineering challenges of ocean liming. Energy, 60,
699 442 -452. https://doi.org/10.1016/j.energy.2013.08.006
700 Renforth, P., Henderson, G. (2017) Assessing ocean alkalinity for carbon sequestration. Reviews of
701 Geophysics, 636-674. doi: 10.1002/2016RG000533
702 Renforth, P., Campbell, J.S. (2021) The role of soils in the regulation of ocean acidification. Phil.
703 Trans. R. Soc. B 376: 20200174. doi: 10.1098/rstb.2020.0174
704 Sarmiento, J. L., Gruber, N. (2006) Ocean Biogeochemical Dynamics. Princeton Univ Pr.
705 Shariatipour, S., Mackay, E., Pickup, G. (2016) An engineering solution for CO_2 injection in saline
706 aquifers. International Journal of Greenhouse Gas Control, 53, 98-105. doi:
707 10.1016/j.ijggc.2016.06.006
708 Shiraki, R., Brantley, S. (1995) Kinetics of near-equilibrium calcite precipitation at 100°C: An
709 evaluation of elementary reaction-based and affinity-based rate laws. Geochimica et
710 Cosmochimica, 59 (8), 1457-1471. doi: 10.1016/0016-7037(95)00055-5
711 Subhas, A., Rollins, N., Berelson, W., Dong, S., Erez, J., Adkins, J. (2015) A novel determination
712 of calcite dissolution kinetics in seawater. Geochimica et Cosmochimica Acta, 170, 51-68. doi:
713 10.1016/j.gca.2015.08.011
714 Sulzer (2021) Static mixers for Water and Wastewater Treatment. Doc. n. 23.83.06.40-IV.06-50

715 Teir, S., Suomalainen, M., Onarheim, K. (2014) Pre-evaluation of a new process for capture of CO_2
716 using water.
717 USGS (2020) PHREEQC Version 3. United States Geological Survey. Retrieved from
718 www.usgs.gov/software/phreeqc-version-3
719 USGS (2021) Crushed Stone Statistics and Information. Minerals Yearbook 2017. United States
720 Geological Survey, National Minerals Information Center. Retrieved from
721 www.usgs.gov/centers/nmic/crushed-stone-statistics-and-information
722 van Heuven S., Pierrot D., Rae J.W.B., Lewis E., Wallace D.W.R. (2011) MATLAB program
723 developed for CO_2 system calculations. ORNL/CDIAC-105b. Oak Ridge, Tennessee, U.S.A:
724 CDIAC, Oak Ridge National Laboratory, Department of Energy.
725 doi:10.3334/CDIAC/otg.CO2SYS_MATLAB_v1.1
726 Zeebe, R. E., Wolf-Gladrow, D. A., Jansen, H. (1999). On the time required to establish chemical
727 and isotopic equilibrium in the carbon dioxide system in seawater. Marine Chemistry, 65, 135-
728 153. doi: 10.1016/S0304-4203(98)00092-9
729
730

SUPPLEMENTARY MATERIAL

Table SM 1: Composition of seawater (Akinsola et al., 2012).

Ion	**molar concentration (mol kg seawater^{-1})**	**mass concentration (g kg seawater^{-1})**
Cl^-	5.459×10^{-1}	19.353
SO_4^{2-}	2.823×10^{-2}	2.712
HCO_3^-	2.327×10^{-3}	0.142
Br^-	1.001×10^{-4}	0.008
F^-	5.263×10^{-5}	0.001
Na^+	4.506×10^{-1}	10.360
Mg^{2+}	5.323×10^{-2}	1.294
Ca^{2+}	1.030×10^{-2}	0.413
K^+	9.898×10^{-3}	0.387
Sr^{2+}	9.130×10^{-5}	0.008
N_3B_3	1.343×10^{-5}	0.001
Total		34.679

Table SM 2: Initial seawater characteristic calculated with CO2SYS and PHREEQC

	Natural seawater calculated with PHREEQC	**Natural seawater calculated with CO2SYS**
pCO_2 (µatm)	420	420
TA (µeq kg^{-1})	2,376	2,200.9
DIC (µmol kg^{-1})	2,327	2,040.8
$CO_{2(aq)}$ (µmol kg^{-1})	30	18.4
HCO_3^- (µmol kg^{-1})	2,221 (*)	1,904.5
CO_3^{2-} (µmol kg^{-1})	76 (*)	117.9
SI_{cal}	0.37	0.44
Ωcal	2.34	2.81
pH	8.0	8.0

(*) These values include the concentration of the free ions and all their ion pairs, e.g. $MgHCO_3^+$

Table SM 3: Kinetics of calcite dissolution in PHREEQC

Code Line	Code statements
1	REM PARM(1)= specific surface area of calcite, cm^2/mol
2	REM PARM(2)=exponent for M/M0
3	si_cc=SI("Calcite")
4	IF(M<=0 and si_cc<0) THEN GOTO 200
5	k1=10^(0.198-440.0/TK)
6	k2=10^(2.84-2177.0/TK)
7	IF TC<=25 THEN k3=10^(-5.86-317.0/TK)
8	IF TC>25 THEN k3=10^(-1.1-1737.0/TK)
9	IF M0>0 THEN area=PARM(1)*M0*(M/M0)^PARM(2) else area=PARM(1)*M
10	rate=area*(k1*ACT("H+")+k2*ACT("CO2")+k3*ACT("H2O"))
11	rate=rate*(1-10^(2/3*si_cc))
12	delta_moles=moles*0.001*TIME
13	SAVE delta_moles
14	END

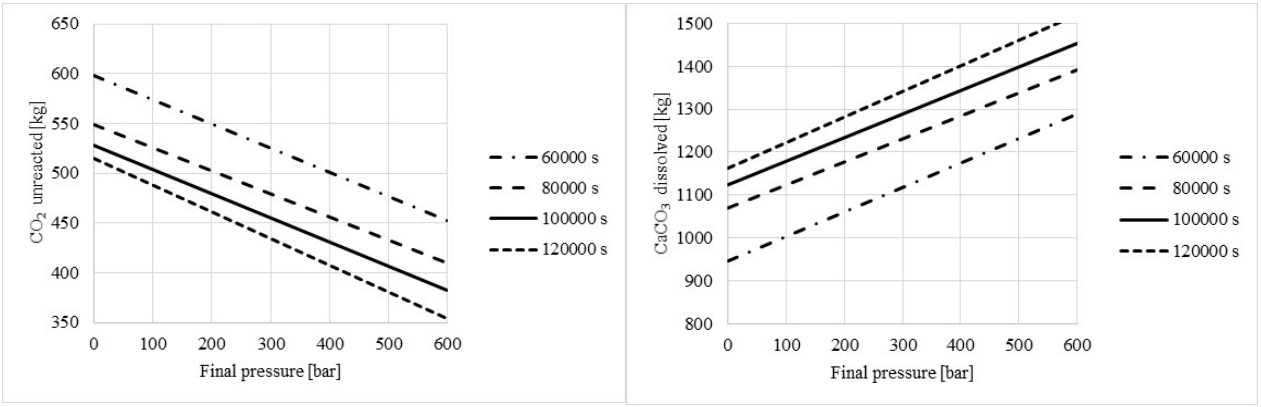

Figure SM 1: Amounts of CO_2 unreacted (left) and maximum amounts of $CaCO_3$ that can dissolve (right) at the end of the pipe for different residence times and different final pressures in the DR, considering 1,500 m^3 of seawater

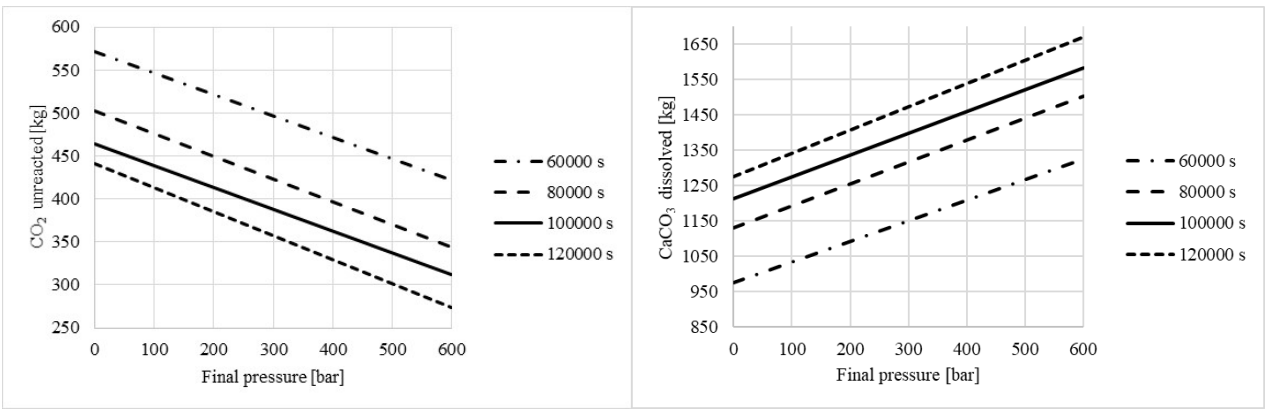

Figure SM 2: Amounts of CO_2 unreacted (left) and maximum amounts of $CaCO_3$ that can dissolve (right) at the end of the pipe for different residence times and different final pressures in the DR, considering 2,500 m^3 of seawater

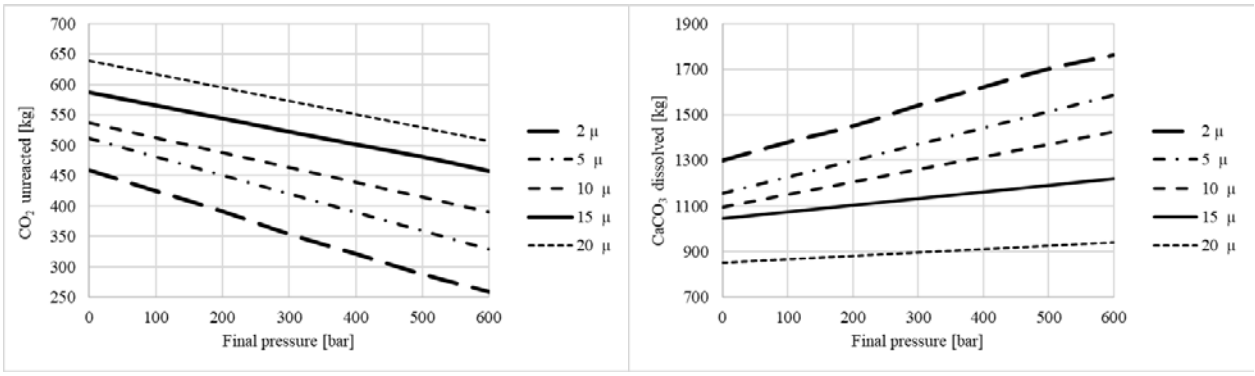

Figure SM 3: Amounts of CO_2 unreacted (left) and maximum amounts of $CaCO_3$ that can dissolve (right) at the end of the pipe for different particle sizes and different final pressures in the DR, considering 1,500 m^3 of seawater

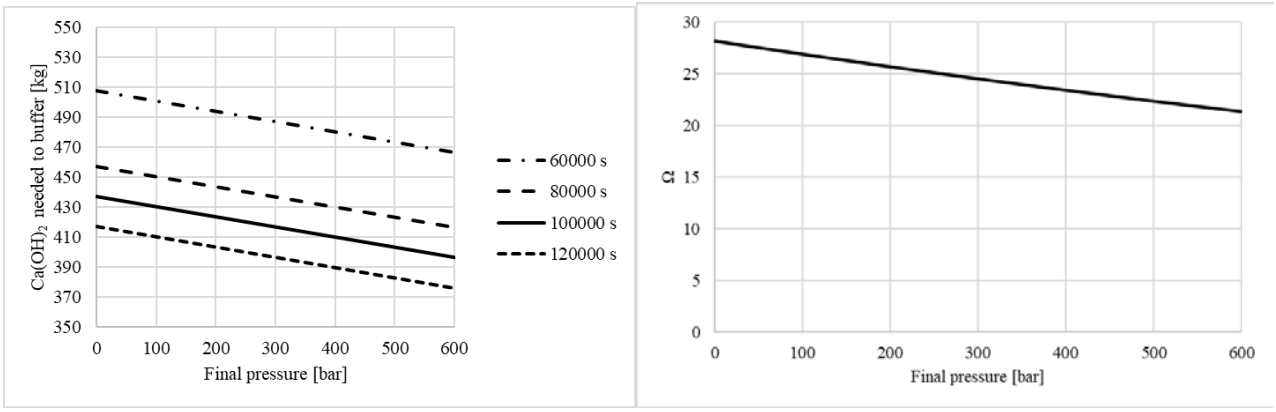

Figure SM 4: Amounts of $Ca(OH)_2$ needed to buffer the unreacted CO_2 (left) and calcite saturation state after the buffering (right) for different residence times and different final pressures, at the end of the BR, considering 1,500 m^3 of seawater

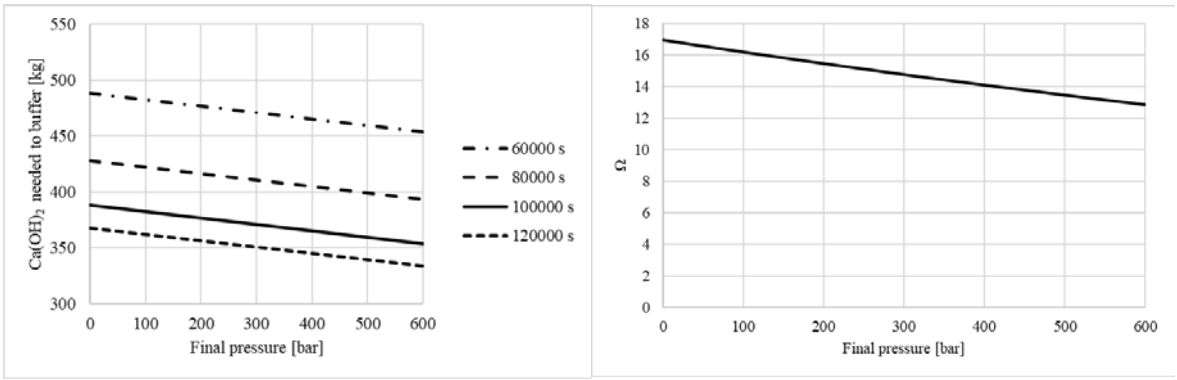

Figure SM 5: Amounts of $Ca(OH)_2$ needed to buffer the unreacted CO_2 (left) and calcite saturation state after the buffering (right) for different residence times and different final pressures, at the end of the BR, considering 2,500 m^3 of seawater

Table SM4: Main electricity consumption in the process, kWh per tCO2 stored coming from an external source

	kWh tCO_2^{-1} net stored
Milling	258
Electric calcination	522
Compressors	89
Pumps	283
Total	1,152

Table SM5: Main component of pipeline CAPEX cost

		quantity	unit	Specific cost € $unit^{-1}$	Total cost (M€)
HDPE resin[1]	DR	103,320	tonne	1000	103
	SL	11,570	tonne		12
Electric energy for extrusion[2]	DR	77,500	MWh	39	3.0
	SL	8,678	MWh		0.34
Ballast[3]	DR	27,360	tonne	300	8.2
	SL	3100	tonne		0.93
Installation[4]	DR + SL	120	km	150,000	18
Industrial margin 25%					36
Total					182

[1]: 120 km of HDPE pipe, OD 3,500 mm, SDR 41
[2]: specific consumption: 750 kWh ton^{-1}
[3]: 25% weigth pipeline displacement
[4]: 2 km/day with 3 ships and 150 workers